Monthly Notices of the ROYAL ASTRONOMICAL SOCIETY

MNRAS **505,** 1600–1606 (2021) https://doi.org/10.1093/mnras/stab1383
Advance Access publication 2021 May 17

GW190814: on the properties of the secondary component of the binary

Bhaskar Biswas,[1]★ Rana Nandi ,[2]★ Prasanta Char,[3] Sukanta Bose[1,4] and Nikolaos Stergioulas[5]

[1]*Inter-University Centre for Astronomy and Astrophysics, Post Bag 4, Ganeshkhind, Pune 411007, India*
[2]*Polba Mahavidyalaya, Hooghly, West Bengal 712148, India*
[3]*Space Sciences, Technologies and Astrophysics Research (STAR) Institute, Université de Liège, Bât. B5a, 4000 Liège, Belgium*
[4]*Department of Physics & Astronomy, Washington State University, 1245 Webster, Pullman, WA 99164-2814, USA*
[5]*Aristotle University of Thessaloniki, Department of Physics, University Campus Laboratory of Astronomy, 54124 Thessaloniki, Greece*

Accepted 2021 May 8. Received 2021 May 1; in original form 2021 February 25

ABSTRACT

We show that the odds of the mass-gap (secondary) object in GW190814 being a neutron star (NS) improve if one allows for a stiff high-density equation of state (EoS) or a large spin. Since its mass is $\in (2.50, 2.67)\,\mathrm{M}_\odot$, establishing its true nature will make it either the heaviest NS or the lightest black hole (BH), and can have far-reaching implications on NS EoS and compact object formation channels. When limiting oneself to the NS hypothesis, we deduce the secondary's properties by using a Bayesian framework with a hybrid EoS formulation that employs a parabolic expansion-based nuclear empirical parametrization around the nuclear saturation density augmented by a generic 3-segment piecewise polytrope (PP) model at higher densities and combining a variety of astrophysical observations. For the slow-rotation scenario, GW190814 implies a very stiff EoS and a stringent constraint on the EoS specially in the high-density region. On the other hand assuming the secondary object is a rapidly rotating NS, we constrain its rotational frequency to be $f = 1170^{+389}_{-495}$ Hz, within a 90 per cent confidence interval (CI). In this scenario, the secondary object in GW190814 would qualify as the fastest rotating NS ever observed. However, for this scenario to be viable, rotational instabilities would have to be suppressed both during formation and the subsequent evolution until merger, otherwise the secondary of GW190814 is more likely to be a BH.

Key words: dense matter – stars: neutron.

1 INTRODUCTION

Recently, the LIGO (Aasi et al. 2015) and Virgo (Acernese et al. 2015) scientific collaborations (LVC) reported the detection of one of the most enigmatic gravitational wave (GW) mergers till date (Abbott et al. 2020a). This event, named GW190814, has been associated with a compact object binary of mass ratio, $q = 0.112^{+0.008}_{-0.009}$, and primary and secondary masses $m_1 = 23.2^{+1.1}_{-1.0}\,\mathrm{M}_\odot$ and $m_2 = 2.59^{+0.08}_{-0.09}$, respectively. Since, an electromagnetic (EM) counterpart has not been found for this particular event and the tidal deformability has not been measurable from the GW signal, the secondary component might well be the lightest BH ever found. However, EM emissions are expected to be observed for only a fraction of NS binaries, and tidal deformabilities are known to be small for massive NSs, hence the secondary in this case cannot be ruled out as an NS. In the latter scenario, it would become the heaviest NS observed in a binary system, given its well-constrained mass. Either hypothesis deserves a deep study owing to its far-reaching implications on the formation channels of such objects and the nature of the densest form of matter in the Universe.

Discoveries of massive pulsars in past decades have severely constrained the EoS of supranuclear matter inside their cores (Demorest et al. 2010; Antoniadis et al. 2013; Fonseca et al. 2016; Arzoumanian et al. 2018; Cromartie et al. 2019). These observations provided a very strong lower bound of $\sim 2\,\mathrm{M}_\odot$ on the maximum mass of non-rotating NSs that all the competing EoS models from nuclear physics must satisfy. Furthermore, GW170817 (Abbott et al. 2017) has prompted several studies predicting an upper bound of $\sim$ 2.2–2.3 $\mathrm{M}_\odot$ on $M_{\max}$ of non-rotating NSs, based on the mass ejecta, kilonova signal and absence of a prompt collapse (Margalit & Metzger 2017; Shibata et al. 2017; Rezzolla, Most & Weih 2018; Ruiz, Shapiro & Tsokaros 2018; Shibata et al. 2019; Shao et al. 2020). While the simultaneous mass−radius measurements of PSR J0030 + 0451 by NICER collaboration (Miller et al. 2019; Riley et al. 2019) indicate a tilt towards slightly stiffer EoS (Biswas et al. 2020; Landry, Essick & Chatziioannou 2020; Raaijmakers et al. 2020), the distribution of m_2 would require even higher $M_{\max}$. Possible formation channels of GW190814-type binaries have also been studied in some recent works (Kinugawa, Nakamura & Nakano 2020; Safarzadeh & Loeb 2020; Zevin et al. 2020). While there is a general consensus that the fallback of a significant amount of bound supernova ejecta on the secondary compact remnant leads to its formation in the lower mass-gap region, the nature of its state at the time of the merger being a BH or an NS remains unclear. Nevertheless, GW190814 has motivated experts to reevaluate the knowledge of dense matter and stellar structure to determine the possible scenarios in which one can construct such configurations of NSs while satisfying relevant constraints (Dexheimer et al. 2020; Fattoyev et al. 2020; Godzieba, Radice & Bernuzzi 2020; Huang et al. 2020; Li, Sedrakian & Weber 2020; Lim et al. 2020; Most et al. 2020; Sedrakian, Weber & Li 2020; Tsokaros, Ruiz & Shapiro 2020; Zhang & Li 2020; Demircik,

★ E-mail:bhaskarb@iucaa.in (BB); nandi.rana@gmail.com (RN)

Ecker & Järvinen 2021; Tews et al. 2021). Most of these works suggest rapid uniform rotation with or without exotic matter, such as hyperons or quark matter, exploiting the caveat that the spin of m_2 is unconstrained. Other possibilities such as m_2 being a primordial BH (Clesse & Garcia-Bellido 2020; Vattis, Goldstein & Koushiappas 2020; Jedamzik 2021), an anisotropic object (Roupas 2021) [see also (Biswas & Bose 2019) for a detailed study on anisotropic object] or a NS in scalar–tensor gravity (Rosca-Mead et al. 2020) have also been considered.

In this article, we investigate the possibility of the GW190814's secondary being a NS within a hybrid nuclear + PP EoS parametrization (Biswas et al. 2020), and study its related properties under assumptions of it being both slowly and rapidly rotating. We also constrain its spin using a universal relation developed by Breu & Rezzolla (2016).

2 A BRIEF REVIEW OF OUR PREVIOUS WORK

In a previous work (Biswas et al. 2020), we have employed Bayesian statistics to constrain the EoS of NS combining multiple astrophysical observations. We have formulated a hybrid nuclear + PP EoS model which uses a parabolic expansion based nuclear empirical parametrization around the nuclear saturation density (ρ_0) and a 3-segment PP parametrization at higher densities. Within the parabolic expansion, the energy per nucleon $e(\rho, \delta)$ of asymmetric nuclear matter can be expressed as

$$e(\rho, \delta) \approx e_0(\rho) + e_{\rm sym}(\rho)\delta^2, \tag{1}$$

where $e_0(\rho)$ is the energy of the symmetric nuclear matter which holds equal number of neutrons and protons. The $e_{\rm sym}(\rho)$ is known as the symmetry energy which characterizes the strength of asymmetry in neutron to proton ratio, and $\delta = (\rho_{\rm n} - \rho_{\rm p})/\rho$ is known as symmetry parameter. $e_0(\rho)$ and $e_{\rm sym}(\rho)$ can be further expanded in a Taylor series around ρ_0:

$$e_0(\rho) = e_0(\rho_0) + \frac{K_0}{2}\chi^2 + ..., \tag{2}$$

$$e_{\rm sym}(\rho) = e_{\rm sym}(\rho_0) + L\chi + \frac{K_{\rm sym}}{2}\chi^2 + ..., \tag{3}$$

where $\chi \equiv (\rho - \rho_0)/3\rho_0$.

At higher densities the EoS of nuclear matter is completely unknown to us. This is the reason we choose a generic 3-segment PP parametrization after $1.25\rho_0$. This particular transition density is motivated by Bayesian evidence calculation which is detailed in Biswas et al. (2020). Then, we construct the posterior of the EoS parameters using Bayesian statistics based on this hybrid nuclear+PP model by combining astrophysical data from the radio observation of PSR J0740 + 6620, GW170817, GW190425, and NICER observations:

$$P(\theta|d) = \frac{P(d|\theta) \times P(\theta)}{P(d)} = \frac{\Pi_i P(d_i|\theta) \times P(\theta)}{P(d)}, \tag{4}$$

where θ is the set of EoS parameters in the model, $d = (d_{\rm GW}, d_{\rm X\text{-}ray}, d_{\rm Radio})$ is the set of data from the three different types of observations that are used to construct the likelihood. The mathematical expressions to compute each of the individual likelihoods are given in equations (5)–(7) of Biswas et al. (2020), respectively.

In this paper, we make use the methodology built in our previous work and investigate the properties of the secondary object of GW190814 under a variety of assumption.

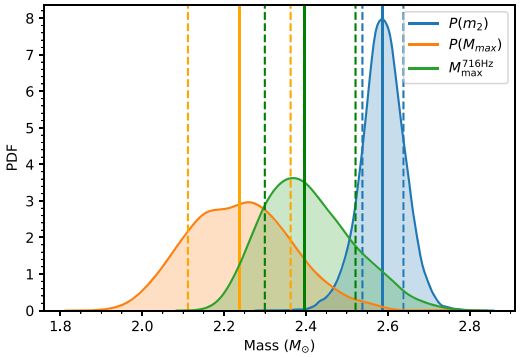

Figure 1. The probability distribution of $M_{\rm max}$ of NSs, obtained from Biswas et al. (2020), is shown in orange. The distribution shown in green is obtained with the same EoS samples as for the orange one, but considering uniform NS rotation at 716 Hz. These two distributions are compared with the probability distribution of the secondary mass m_2 (in blue) deduced from the GW190814 posterior samples in Abbott et al. (2020b).

3 LIGHTEST BH OR HEAVIEST NS?

The mass of the secondary object in GW190814 measured by the LVC falls into the so-called 'mass gap' region (Bailyn et al. 1998; Özel et al. 2010) and therefore demands a careful inspection of its properties before it can be ruled out as a BH or NS.

A non-informative measurement of the tidal deformability or the spin of the secondary, or the absence of an EM counterpart associated with this event, has made it difficult to make a robust statement about the nature of this object. We begin by examining if the GW mass measurement along with hybrid nuclear + PP model alone can rule it out as an NS. In Fig. 1, the posterior distribution of secondary mass m_2 is plotted, in blue, by using publicly available LVC posterior samples (Abbott et al. 2020b) .[1] In orange, the posterior distribution of $M_{\rm max}$ is overlaid from hybrid nuclear + PP model analysis by Biswas et al. (2020) using PSR J0740+6620 (Cromartie et al. 2019), combined GW170817[2] (Abbott et al. 2018) and GW190425 (Abbott et al. 2020a),[3] and NICER[4] data.

Given these two distributions – both for non-rotating stars – we calculate the probability of m_2 being greater than $M_{\rm max}$, i.e. $P(m_2 > M_{\rm max}) = P(m_2 - M_{\rm max})$. This probability can be easily obtained by calculating the convolution of the m_2 and $-M_{\rm max}$ probability distributions, which yields $P(m_2 > M_{\rm max}) = 0.99$. Therefore, the mass measurement implies that the probability that the secondary object in GW190814 is an NS is ~ 1 per cent. However, this type of analysis is highly sensitive to the choice of EoS parametrization as well as on the implementation of the maximum-mass constraint obtained from the heaviest pulsar observations. The LVC analysis (Abbott et al. 2020b) that is based on the spectral EoS parametrization (Lindblom 2010), obtained ~ 3 per cent probability for the secondary to be an NS using GW170817-informed EoS samples from Abbott et al. (2018). The addition of NICER data might increase this probability. Essick & Landry (2020) added NICER data in their analysis of GW observations based on a non-parametric EoS and also examined the impact of different assumptions about the compact object mass distribution. The $P(m_2 > M_{\rm max})$ probabilities technically depend on

[1]LVK collaboration, https://dcc.ligo.org/LIGO-P2000183/public
[2]LVK collaboration, https://dcc.ligo.org/LIGO-P1800115/public
[3]LVK collaboration, https://dcc.ligo.org/LIGO-P2000026/public
[4]PSR J0030 + 0451 mass–radius samples released by Miller et al. (2019), https://zenodo.org/record/3473466#.XrOt1nWlxBc

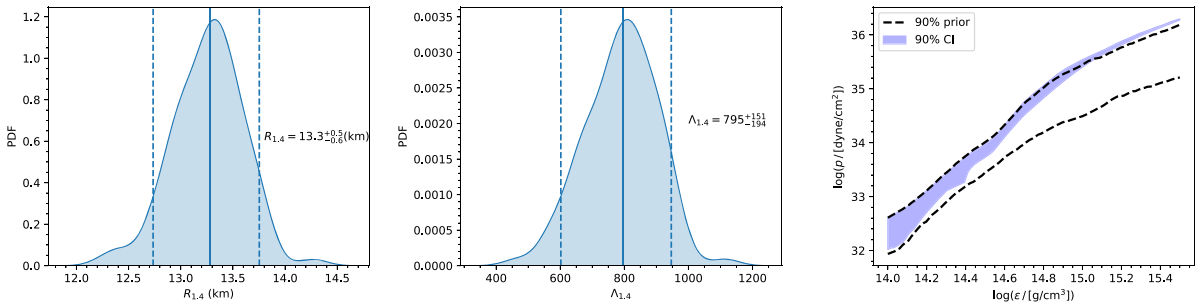

Figure 2. Posterior distributions of $R_{1.4}$ (left-hand panel) and $\Lambda_{1.4}$ (middle panel), as well as the pressure as a function of energy density (right-hand panel) are plotted assuming that the secondary companion of GW190814 is a non-rotating NS. Median and 90 per cent CI are shown by solid and dashed lines, respectively.

the mass prior assumed for the secondary, but Essick et al. (2020) showed that, regardless of assumed population model, there is a less than ~ 6 per cent probability for the GW190814 secondary to be an NS. In the discovery paper, LVC also reported an EoS-independent result using the pulsar mass distribution, following Farr & Chatziioannou (2020), which suggests that there is less than ~ 29 per cent probability that the secondary is an NS. Despite the differences inherent to these studies, they all suggest that there is a small but finite probability of the secondary object in GW190814 to be an NS. It is also important to note that they all assumed the NS to be either non-rotating or slowly rotating ($\chi < 0.05$).

Another possibility is that the secondary object is a rapidly rotating NS (Most et al. 2020; Tsokaros et al. 2020). It is known that uniform rotation can increase the maximum mass of an NS by ~ 20 per cent (Friedman & Ipser 1987; Cook, Shapiro & Teukolsky 1992, 1994). Therefore, rapid rotation may improve the chances that the GW190814 data are consistent with an NS.

From pulsar observations, we know that NSs with spin frequencies as high as $\nu_{\rm max}^{\rm obs} = 716$ Hz exist in nature (Hessels et al. 2006). Using this value for the spin frequency and the EoS samples of Biswas et al. (2020), we can deduce the maximum improvement in probability that the GW190814 secondary is an NS. We used this information in the `RNS` code (Stergioulas & Friedman 1995) and obtained a corresponding distribution of maximum mass denoted as $M_{\rm max}^{\rm 716Hz}$. The superscript '716 Hz' emphasizes that all configurations here are computed at that fixed spin frequency. In Fig. 1, the distribution of $M_{\rm max}^{\rm 716Hz}$ is shown in green. From the overlap of this distribution with $P(m_2)$, we find there is ~ 8 per cent probability that m_2 is a rapidly rotating NS.

Alternatively, if the GW190814's secondary were indeed an NS, then the LVC mass measurement sets a lower limit on the maximum NS mass for any spin at least up to $\nu_{\rm max}^{\rm obs}$.

We next relax this constraint by considering all theoretically allowed values of the spin frequency, which for some masses and EoSs may exceed the maximum observed value. In the next two sections, we investigate the properties of NSs – for various rotational frequencies – using a Bayesian approach based on hybrid nuclear + PP EoS parametrization.

4 PROPERTIES ASSUMING A SLOWLY ROTATING NS

For slowly rotating NS, a Bayesian methodology was already developed in Biswas et al. (2020) (also briefly described in Section 2) by combining multiple observations based on hybrid nuclear + PP EoS parametrization. In this paper, instead of marginalizing over the mass of PSR J0740+6620 taking into account of its measurement uncertainties (as described in Biswas et al. 2020), we consider the m_2 distribution of GW190814 as the heaviest pulsar mass measurement. We use Gaussian kernel-density to approximate the posterior distribution of m_2. The resulting posteriors of radius ($R_{1.4}$) and tidal deformability ($\Lambda_{1.4}$) obtained from this analysis are plotted in Fig. 2. We find that $R_{1.4} = 13.3^{+0.5}_{-0.6}$ km and $\Lambda_{1.4} = 795^{+151}_{-194}$, at 90 per cent CI, which are in good agreement with previous studies (Abbott et al. 2020a; Essick & Landry 2020; Tews et al. 2021).

The addition of GW190814 makes the EoS stiffer, especially in the high-density region since now a very small subspace of the EoS family can support an $\sim 2.6\,{\rm M}_\odot$ NS. In the right-hand panel of Fig. 2, the 90 per cent CI of posterior of the pressure inside the NS is plotted as a function of energy density in shaded blue colour and the corresponding 90 per cent CI of prior is shown by the black dotted lines. This plot clearly shows that the addition of GW190814 places a very tight constraint on the high-density part of the EoS.

5 PROPERTIES ASSUMING A RAPIDLY ROTATING NS

In this article, for the first time, we develop a Bayesian formalism to constrain the EoS of NS that allows for rapid rotation. We use a universal relation found by Breu & Rezzolla (2016) which relates the maximum mass of a uniformly rotating star ($M_{\rm rmax}^{\rm rot}$) with the maximum mass of a non-rotating star ($M_{\rm max}^{\rm TOV}$) for the same EoS

$$M_{\rm rmax}^{\rm rot} = M_{\rm max}^{\rm TOV}\left[1 + a_1\left(\frac{\chi}{\chi_{\rm kep}}\right)^2 + a_2\left(\frac{\chi}{\chi_{\rm kep}}\right)^4\right], \quad (5)$$

where $a_1 = 0.132$ and $a_2 = 0.071$. χ is the dimensionless spin magnitude of a uniformly rotating star and $\chi_{\rm kep}$ is the maximum allowed dimensionless spin magnitude at the mass-shedding limit. Given a $\chi/\chi_{\rm kep}$ value, we calculate $M_{\rm rmax}^{\rm rot}$ using this universal relation. Its use makes our computation much faster but can cause up to ~ 2 per cent deviation from the exact result, as noted by Breu & Rezzolla (2016). We assume that the error is constant throughout the parameter space; we took it to be distributed uniformly in [−2 per cent, 2 per cent] and marginalized over it to get an unbiased estimate of the properties of the object.

We combine data from PSR J0740 + 6620, two other binary neutron stars, namely GW170817 and GW190425, as well as NICER data assuming non-rotating NS following Biswas et al. (2020). Then, the m_2 distribution of GW190814 is used for the maximum-mass threshold of a uniformly rotating star, i.e. $M_{\rm rmax}^{\rm rot}$. We use a nested sampler algorithm implemented in `Pymultinest` (Buchner et al. 2014) to simultaneously sample the EoS parameters and $\chi/\chi_{\rm kep}$. These posterior samples are then used in the `RNS` code (Stergioulas &

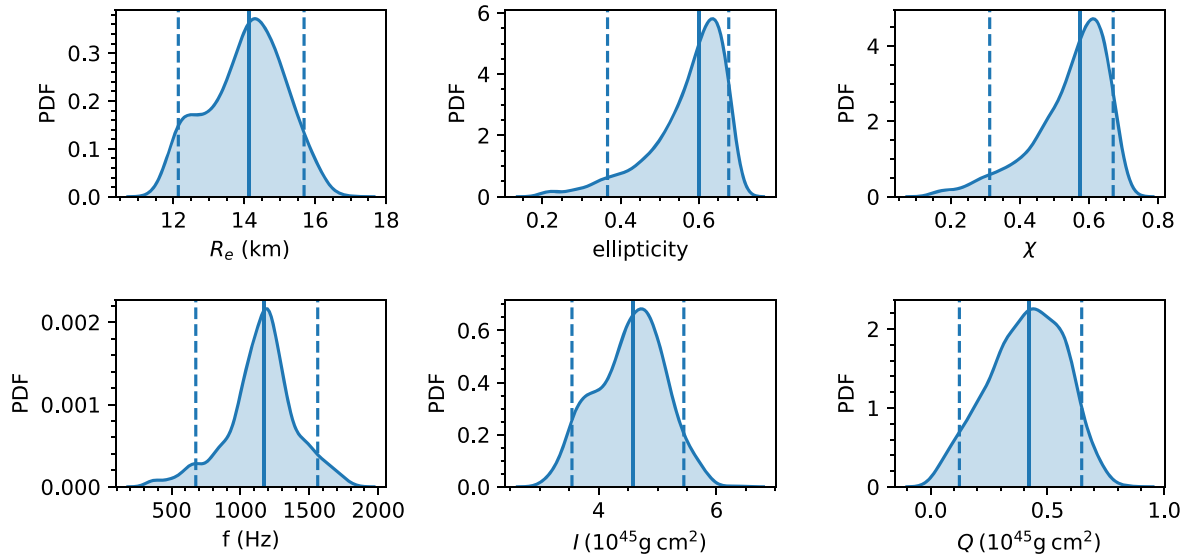

Figure 3. Posterior distribution of various properties of the secondary companion of GW190814 is shown assuming a rapidly rotating NS: Equatorial radius R_e (upper left), ellipticity e (upper middle), dimensionless spin magnitude χ (upper right), rotational frequency f in Hz (lower left), moment of Inertia I (lower middle), and quadrupole moment Q (lower right). Median and 90 per cent CI are shown by solid and dashed lines, respectively.

Friedman 1995) to calculate several properties of the secondary object associated with GW190814.

In the upper left and middle panel of Fig. 3 posterior distributions of equatorial radius (R_e) and ellipticiy (e) are plotted, respectively. Within the 90 per cent CI we find $R_e = 14.1^{+1.5}_{-2.0}$ km and $e = 0.60^{+0.07}_{-0.23}$. Such high values of equatorial radius and ellipticity imply a considerable deviation from a spherically symmetric static configuration. From the distribution of χ shown in the upper left panel of Fig. 3 we find its value to be $\chi = 0.57^{+0.09}_{-0.26}$. Most et al. (2020) have also obtained a similar bound on χ with simpler arguments. In this paper, we provide a distribution for χ employing a Bayesian framework as well as place a more robust bound on this parameter. In the lower left panel of Fig. 3, the posterior distribution of rotational frequency is plotted in Hz. We find its value to be $f = 1170^{+389}_{-495}$ Hz. As noted above, till date PSR J1748−2446a (Hessels et al. 2006) is known as the fastest rotating pulsar, with a rotational frequency of 716 Hz. *Therefore, if the secondary of GW190814 is indeed a rapidly rotating NS, it would definitely be the fastest rotating NS observed so far.* In the lower middle and right-hand panels, the posterior distributions of the moment of inertia and quadrupole moment of the secondary are shown, respectively.

5.1 Maximum spin frequencies and rotational instabilities

EoS constraints derived from the observation of non-rotating NSs also provide an upper bound on the maximum spin of an NS. The maximum spin frequency is given empirically as $f_{\rm lim} \simeq \frac{1}{2\pi}(0.468 + 0.378\chi_s)\sqrt{\frac{GM_{\rm max}}{R^3_{\rm max}}}$, (Lasota, Haensel & Abramowicz 1996; Paschalidis & Stergioulas 2017) where $\chi_s = \frac{2GM_{\rm max}}{R_{\rm max}c^2}$, with $M_{\rm max}$ and $R_{\rm max}$ being the maximum mass and its corresponding radius of a non-rotating NS, respectively. We use $M_{\rm max}$–$R_{\rm max}$ posterior samples that were deduced in Biswas et al. (2020) by using PSR J0740 + 6620, combined GWs, and NICER data to calculate $f_{\rm lim}$. In the left-hand panel of Fig. 4, its distribution is shown by the grey-shaded region. We overlay that distribution with distributions of frequencies of the secondary object of GW190814 and those of a few hypothetical rotating NSs of various masses – all Gaussian distributed, but with medians of 2.4, 2.8, and 3.0 $M_\odot$, respectively, and each having a measurement uncertainty of 0.1 $M_\odot$. We also assume the primary component of GW190425 to be a rapidly rotating NS, since by using a high-spin prior LVC determined its mass to be 1.61–2.52 $M_\odot$. In our calculations, for GW190425 we used the publicly available high-spin posterior of m_1 obtained by using the PhenomPNRT waveform. We find observations like m_1 of GW190425 and simulations like $\mathcal{N}(2.4, 0.1\,M_\odot)$ correspond to posteriors of rotational frequency that are comparatively lower than limiting values of rotational frequencies. However, as the mass increases, the posterior of frequency eventually almost coincides with $f_{\rm lim}$. Therefore, if the secondary of GW190814 was a rapidly rotating NS, it would have to be rotating rather close to the limiting frequency.

Any rotating star is generically unstable through the Chandrasekhar–Friedman–Schutz (CFS) mechanism (Chandrasekhar 1970; Friedman & Schutz 1978). This instability occurs when a certain retrograde mode in the rotating frame becomes prograde in the inertial frame. For example, the f modes of a rotating NS can always be made unstable for a sufficiently large mode number m (not to be confused with component masses $m_{1,2}$) even for low-spin frequencies, but, the instability time-scale increases rapidly with the increase of m. Numerical calculations have shown (Stergioulas & Friedman 1998; Morsink, Stergioulas & Blattnig 1999), that for maximum mass stars $m = 2$ mode changes from retrograde to prograde at $T/|W| \sim 0.06$, where T is the rotional energy and W the gravitational potential energy of the NS. We computed this ratio for all the cases considered in this section and plot the distributions in the right-hand panel of Fig. 4. From this analysis, we find that the secondary of GW190814 should be f mode unstable as for most of the allowed EoSs $T/|W|$ is significantly larger than 0.06. The CFS instability is even more effective for r modes (Lindblom, Owen & Morsink 1998; Andersson, Kokkotas & Schutz 1999) as they are generically unstable for all values of spin frequency. However, an instability can develop, only if its growth time-scale is shorter than the time-scale of the strongest damping mechanism affecting it. A multitude of damping mechanisms, such

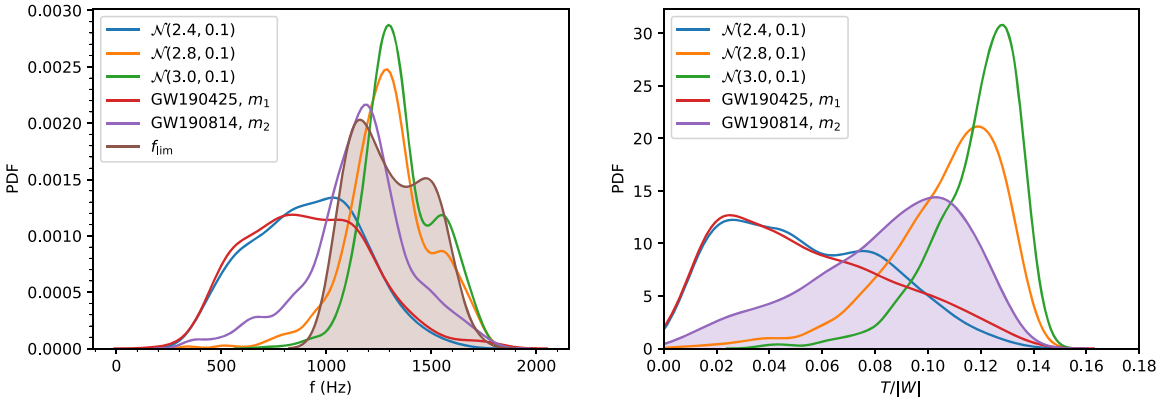

Figure 4. In the left-hand panel, the probability distribution of $f_{\rm lim}$ is shown in brown shade. The distribution of $f_{\rm lim}$ is plotted considering three simulated rapidly rotating NS whose mass measurements are Gaussian distributed with median 2.4, 2.8, and 3.0 $M_\odot$, respectively, and each having a measurement uncertainty of 0.1 $M_\odot$. The same has been overlaid using the secondary component of the GW190814 and the primary of the GW190425 events. In the right-hand panel, the corresponding ratio of rotational to gravitational potential energy $T/|W|$ is shown.

as shear viscosity, bulk viscosity, viscous boundary layer, crustal resonances, and superfluid mutual friction (each having each own temperature dependence) have been investigated (see Kokkotas & Schwenzer 2016; Paschalidis & Stergioulas 2017; Andersson 2019; Zhou, Li & Li 2021 and references therein). The spin distribution of millisecond pulsars in accreting systems (Papitto et al. 2014) can be explained, if the r mode instability is effectively damped up to spin frequencies of ~ 700 Hz (Ho, Andersson & Haskell 2011), and operating at higher spin rates. This would not allow for the secondary in GW190814 to be a rapidly rotating NS at the limiting spin frequency.

On the other hand, if the secondary of GW190814 *was* a rapidly rotating NS at the limiting frequency, then the f-mode and r-mode instabilities must be effectively damped both during the spin-up phase in a low-mass X-ray binary, where it acquires rapid rotation, as well as during its subsequent lifetime up to the moment of merger. This might be possible, if both the f-mode and the r-mode instabilities are damped by a particularly strong mutual friction of superfluid vortices below the superfluid transition temperature of $\sim 10^9$ K (see Lindblom & Mendell 2000; Gaertig et al. 2011 and in particular the case of an intermediate drag parameter $\mathcal{R} \sim 1$ in Haskell, Andersson & Passamonti 2009). If this is the case, then the limiting frequency observed in the spin distribution of millisecond pulsars must be explained by other mechanisms (see Gittins & Andersson 2019). A possible presence of rapidly rotating NS in merging binaries thus would have strong implications on the physics of superfluidity in NS matter (in particular constraining the drag parameter $\mathcal{R}$ of mutual friction) and on the astrophysics of accreting systems.

6 CONSTRAINING NS EOS ASSUMING THAT THE GW190814 SECONDARY IS A BH

So far, we have analysed the impact on NS EoS properties arising from the hypothesis that the secondary object in GW190814 is an NS. On the other hand, if that secondary object is a BH, then again novel information about the NS EoS can be obtained, since it will set an upper bound on the NS maximum mass, but only if one were to assume that the NS and BH mass distributions do not overlap.

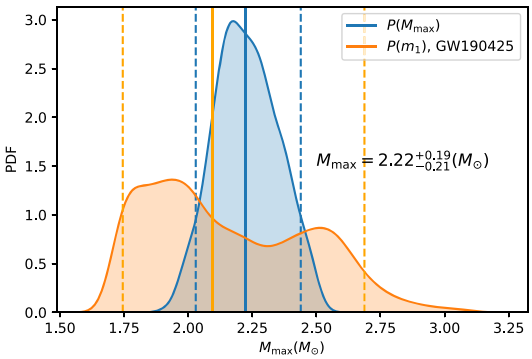

Figure 5. The probability of NS $M_{\rm max}$ is plotted in blue, under the hypothesis that the GW190814 secondary is a BH. Overlaid in orange is the LVC posterior of the primary in GW190425, for the high-spin prior.

In our analysis, we take this value to be 2.5 $M_\odot$, which is the lowest possible value of the secondary object within 90 per cent CI. Then, using Bayesian inference for non-rotating stars, we combine PSR J0740+6620, GWs, and NICER data to place further constraints on the NS EoS. In Fig. 5, the distribution of the maximum mass for non-rotating NSs is shown in blue using the EoS samples obtained from this analysis. Within the 90 per cent CI we find $M_{\rm max} = 2.22^{+0.19}_{-0.21}\,M_\odot$, which is the most conservative bound on NS maximum mass obtained so far in this work.

Assuming a high-spin prior, the mass of the primary component of GW190425 is constrained between $1.61-2.52\,M_\odot$. In Fig. 5, its distribution is overplotted in orange. From the overlap with the newly obtained $M_{\rm max}$ distribution and the m_1 distribution of GW190425, we find that there is ~ 40 per cent probability that the primary of GW190425 is a BH.

7 CONCLUSION

Based on the maximum mass samples obtained from Biswas et al. (2020), we find that there is ~ 1 per cent probability that the secondary object associated with GW190814 is a non-rotating NS. However, such an estimation depends on the choice of EoS parametrization and the maximum mass threshold. Nevertheless,

the possibility of the secondary being a non-rotating NS is not inconsistent with the data. Based on our hybrid nuclear + PP EoS parametrization, we find that the addition of GW190814 as a non-rotating stars provides a very stringent constraint on the EoS specially in the high-density region. We also discussed the alternative that the secondary is a rapidly rotating NS. We find that in order to satisfy the secondary mass estimate of GW190814, its spin magnitude has to be close to the limiting spin frequency for uniform rotation. In fact, it would be the fastest rotating NS ever observed. However, this could be the case, only if gravitational-wave instabilities are effectively damped for rapidly rotating stars, which opens the possibility of constraining physical mechanisms, such as mutual friction in a superfluid interior.

ACKNOWLEDGEMENTS

We thank Philippe Landry and Toni Font for carefully reading the manuscript and making several useful suggestions. We gratefully acknowledge the use of high performance super-computing cluster Pegasus at IUCAA for this work. PC is supported by the Fonds de la Recherche Scientifique-FNRS, Belgium, under grant No. 4.4503.19. This research has made use of data, software and/or web tools obtained from the Gravitational Wave Open Science Center (https://www.gw-openscience.org), a service of the LIGO (Laser Interferometer Gravitational-Wave Observatory) Laboratory, the LIGO Scientific Collaboration and the Virgo Collaboration. LIGO is funded by the U.S. National Science Foundation. The authors gratefully acknowledge the Italian Istituto Nazionale di Fisica Nucleare (INFN), the French Centre National de la Recherche Scientifique (CNRS) and the Netherlands Organization for Scientific Research, for the construction and operation of the Virgo detector and the creation and support of the EGO (European Gravitational Observatory) consortium. We would like to thank all of the essential workers who put their health at risk during the COVID-19 pandemic, without whom we would not have been able to complete this work.

NOTE ADDED IN PROOF

Recently the mass of PSR J0740+6620 was revised slightly downwards – to $2.08^{+0.07}_{-0.07}\,M_{\odot}$, at 68 per cent CI (Fonseca et al. 2021). This has a marginal effect on the EoS posterior, potentially making some slightly softer EoSs viable (Biswas 2021). Consequently, under the rapidly rotating scenario, the spin of the secondary would become slightly higher than what is reported in this paper.

DATA AVAILABILITY

The data generated in this article will be shared on reasonable request to the corresponding author.

REFERENCES

Aasi J. et al., 2015, Class. Quantum Gravity, 32, 074001
Abbott B. P. et al., 2017, Phys. Rev. Lett., 119, 161101
Abbott B. P. et al., 2018, Phys. Rev. Lett., 121, 161101
Abbott R. et al., 2020a, ApJ, 892, L3
Abbott R. et al., 2020b, ApJ, 896, L44
Acernese F. et al., 2015, Class. Quantum Gravity, 32, 024001
Andersson N., 2019, Gravitational-Wave Astronomy: Exploring the Dark Side of the Universe. Oxford Graduate Texts, Oxford Univ. Press, Oxford
Andersson N., Kokkotas K., Schutz B. F., 1999, ApJ, 510, 846
Antoniadis J. et al., 2013, Science, 340, 6131
Arzoumanian Z. et al., 2018, ApJS, 235, 37
Bailyn C. D., Jain R. K., Coppi P., Orosz J. A., 1998, ApJ, 499, 367
Biswas B., 2021, preprint(arXiv:2105.02886)
Biswas B., Bose S., 2019, Phys. Rev. D, 99, 104002
Biswas B., Char P., Nandi R., Bose S., 2021, Phys. Rev. D, 103, 103015
Breu C., Rezzolla L., 2016, MNRAS, 459, 646
Buchner J. et al., 2014, A&A, 564, A125
Chandrasekhar S., 1970, Phys. Rev. Lett., 24, 611
Clesse S., Garcia-Bellido J., 2020, preprint(arXiv:2007.06481)
Cook G. B., Shapiro S. L., Teukolsky S. A., 1992, ApJ, 398, 203
Cook G. B., Shapiro S. L., Teukolsky S. A., 1994, ApJ, 424, 823
Cromartie H. T. et al., 2019, Nat. Astron., 4, 72
Demircik T., Ecker C., Järvinen M., 2021, ApJ, 907, L37
Demorest P., Pennucci T., Ransom S., Roberts M., Hessels J., 2010, Nature, 467, 1081
Dexheimer V., Gomes R. O., Klähn T., Han S., Salinas M., 2021, Phys. Rev. C, 103, 025808
Essick R., Landry P., 2020, ApJ, 904, 80
Essick R., Tews I., Landry P., Reddy S., Holz D. E., 2020, Phys. Rev. C, 102, 055803
Farr W. M., Chatziioannou K., 2020, Res. Notes Am. Astron. Soc., 4, 65
Fattoyev F. J., Horowitz C. J., Piekarewicz J., Reed B., 2020, Phys. Rev. C, 102, 065805
Fonseca E. et al., 2016, ApJ, 832, 167
Fonseca E. et al., 2021, preprint(arXiv:2104.00880)
Friedman J. L., Ipser J. R., 1987, ApJ, 314, 594
Friedman J. L., Schutz B. F., 1978, ApJ, 222, 281
Gaertig E., Glampedakis K., Kokkotas K. D., Zink B., 2011, Phys. Rev. Lett., 107, 101102
Gittins F., Andersson N., 2019, MNRAS, 488, 99
Godzieba D. A., Radice D., Bernuzzi S., 2020, ApJ, 908, 122
Haskell B., Andersson N., Passamonti A., 2009, MNRAS, 397, 1464
Hessels J. W., Ransom S. M., Stairs I. H., Freire P. C. C., Kaspi V. M., Camilo F., 2006, Science, 311, 1901
Ho W. C. G., Andersson N., Haskell B., 2011, Phys. Rev. Lett., 107, 101101
Huang K., Hu J., Zhang Y., Shen H., 2020, ApJ, 904, 39
Jedamzik K., 2021, Phys. Rev. Lett., 126, 051302
Kinugawa T., Nakamura T., Nakano H., 2021, PTEP, 2021, 021E01
Kokkotas K. D., Schwenzer K., 2016, Eur. Phys. J. A, 52, 38
Landry P., Essick R., Chatziioannou K., 2020, Phys. Rev. D, 101, 123007
Lasota J.-P., Haensel P., Abramowicz M. A., 1996, ApJ, 456, 300
Li J. J., Sedrakian A., Weber F., 2020, Phys. Lett. B, 810, 135812
Lim Y., Bhattacharya A., Holt J. W., Pati D., 2020, preprint(arXiv:2007.06526)
Lindblom L., 2010, Phys. Rev., D82, 103011
Lindblom L., Mendell G., 2000, Phys. Rev. D, 61, 104003
Lindblom L., Owen B. J., Morsink S. M., 1998, Phys. Rev. Lett., 80, 4843
Margalit B., Metzger B. D., 2017, ApJ, 850, L19
Miller M. C. et al., 2019, ApJ, 887, L24
Morsink S. M., Stergioulas N., Blattnig S. R., 1999, ApJ, 510, 854
Most E. R., Papenfort L. J., Weih L. R., Rezzolla L., 2020, MNRAS, 499, L82
Özel F., Psaltis D., Narayan R., McClintock J. E., 2010, ApJ, 725, 1918
Papitto A., Torres D., Rea N., Tauris T., 2014, A&A, 566, A64
Paschalidis V., Stergioulas N., 2017, Living Rev. Rel., 20, 7
Raaijmakers G. et al., 2020, ApJ, 893, L21
Rezzolla L., Most E. R., Weih L. R., 2018, ApJ, 852, L25
Riley T. E. et al., 2019, ApJ, 887, L21
Rosca-Mead R., Moore C. J., Sperhake U., Agathos M., Gerosa D., 2020, Symmetry, 12, 1384
Roupas Z., 2021, Ap&SS, 366, 9
Ruiz M., Shapiro S. L., Tsokaros A., 2018, Phys. Rev. D, 97, 021501
Safarzadeh M., Loeb A., 2020, ApJ, 899, L15
Sedrakian A., Weber F., Li J. J., 2020, Phys. Rev. D, 102, 041301
Shao D.-S., Tang S.-P., Sheng X., Jiang J.-L., Wang Y.-Z., Jin Z.-P., Fan Y.-Z., Wei D.-M., 2020, Phys. Rev. D, 101, 063029

Shibata M., Fujibayashi S., Hotokezaka K., Kiuchi K., Kyutoku K., Sekiguchi Y., Tanaka M., 2017, Phys. Rev. D, 96, 123012
Shibata M., Zhou E., Kiuchi K., Fujibayashi S., 2019, Phys. Rev. D, 100, 023015
Stergioulas N., Friedman J., 1995, ApJ, 444, 306
Stergioulas N., Friedman J. L., 1998, ApJ, 492, 301
Tews I., Pang P. T. H., Dietrich T., Coughlin M. W., Antier S., Bulla M., Heinzel J., Issa L., 2021, ApJ, 908, L1
Tsokaros A., Ruiz M., Shapiro S. L., 2020, ApJ, 905, 48
Vattis K., Goldstein I. S., Koushiappas S. M., 2020, Phys. Rev. D, 102, 061301
Zevin M., Spera M., Berry C. P., Kalogera V., 2020, ApJ, 899, L1
Zhang N.-B., Li B.-A., 2020, ApJ, 902, 38
Zhou X., Li A., Li B.-A., 2021, ApJ, 910, 62

This paper has been typeset from a TEX/LATEX file prepared by the author.